Dense water formation on the northwestern shelf of the Okhotsk Sea: 1. Direct observations of brine rejection

Andrey Y. Shcherbina, Lynne D. Talley, and Daniel L. Rudnick
Scripps Institution of Oceanography, University of California, San Diego, La Jolla, California, USA

Received 10 November 2003; revised 19 March 2004; accepted 21 April 2004; published 1 July 2004.

[1] Dense Shelf Water (DSW) formation due to brine rejection in the coastal polynya on the northwestern shelf of the Okhotsk Sea was studied using two bottom moorings during the winter of 1999–2000. A steady salinity and density increase that continued for over a month was observed at the shallower mooring. The maximum density of σ_θ = 26.92 kg m^{-3} was reached during this period. The density increase terminated abruptly in late February, while the active brine rejection continued for several more weeks based on indirect evidence from water properties and ice cover. This termination was possibly due to the onset of baroclinic instability of the density front at the polynya edge facilitating offshore eddy transport of the density anomaly. Observed periodic baroclinic tide intensification events are hypothesized to be an indicator of the presence of such baroclinic eddies. No significant density increase was observed at the deeper, offshore mooring, indicating a robust demarcation of the offshore extent of newly formed DSW. The relatively fresh water of the tidally mixed zone inshore of the shelf front was the precursor of the DSW, aided by the late-autumn offshore transition of the front. *INDEX TERMS:* 4207 Oceanography: General: Arctic and Antarctic oceanography; 4219 Oceanography: General: Continental shelf processes; 4540 Oceanography: Physical: Ice mechanics and air/sea/ice exchange processes; 4243 Oceanography: General: Marginal and semienclosed seas; *KEYWORDS:* Okhotsk Sea, brine rejection, dense water formation

Citation: Shcherbina, A. Y., L. D. Talley, and D. L. Rudnick (2004), Dense water formation on the northwestern shelf of the Okhotsk Sea: 1. Direct observations of brine rejection, *J. Geophys. Res.*, *109*, C09S08, doi:10.1029/2003JC002196.

1. Introduction

[2] The Okhotsk Sea is a marginal sea in the subpolar gyre of the northwestern Pacific (Figure 1a). It is separated from the open ocean by the chain of Kuril Islands with several fairly deep straits between them. Net inflow of the water through the deepest northern strait, Kruzenshtern (1.9 km deep), and net outflow through the deepest Bussol' Strait (2.3 km deep), combined with positive windstress curl, sets the general cyclonic circulation in the basin [*Ohshima et al.*, 2004].

[3] A combination of harsh wintertime conditions, wide shelves, and relatively high background salinities makes the Okhotsk Sea the principal ventilation site for the intermediate density waters of the North Pacific [*Talley*, 1991]. This overturn is driven by brine rejection, accompanying ice formation on the northern shelves of the sea.

[4] Seasonal ice cover extends virtually over the whole basin during the winter; however, no multiyear ice is present. Prevailing offshore winds create several fairly large and persistent polynyas along the northern and northwestern coasts (Figure 1b). Rapid frazil ice formation in the polynyas leads to brine rejection and formation of dense shelf water (DSW) in these regions [*Kitani*, 1973; *Alfultis and Martin*, 1987; *Martin et al.*, 1998; *Gladyshev et al.*, 2000]. Subsequently, this cold, oxygen-rich, but relatively fresh water is advected southward along the coast of Sakhalin island and through Bussol' Strait into open ocean. Along the way it undergoes significant modification through mixing and entertainment, forming Okhotsk Sea Mode Water (OSMW) [*Yasuda*, 1997; *Gladyshev et al.*, 2003]. Ultimately, OSMW provides the low-salinity and high-oxygen features of the North Pacific Intermediate Water (NPIW), marking the highest ventilated density levels in the North Pacific [*Talley*, 1991].

[5] Of all the polynyas contributing to OSMW, only the one located on the northwestern shelf produces the densest water (26.8–27.2 σ_θ), with density reaching that of NPIW [*Kitani*, 1973; *Gladyshev et al.*, 2000]. The special role of the northwestern polynya (NWP) is likely due to its downstream location with respect to the other northern shelf polynyas, which allows the NWP to augment the brine accumulation started upstream.

[6] Owing to the difficulty of wintertime access, all past information regarding the details of DSW formation in the Okhotsk Sea polynyas was derived from satellite remote sensing, warm season in situ observations, and water mass analyses. The present paper summarizes the results of the first direct observation of brine rejection on the northwestern shelf of the Okhotsk Sea, obtained with bottom moorings during the winter of 1999–2000. These observations were described briefly by *Shcherbina et al.* [2003]. Section 2 presents the hydrographic and mooring data used in the

0148-0227/04/2003JC002196$09.00

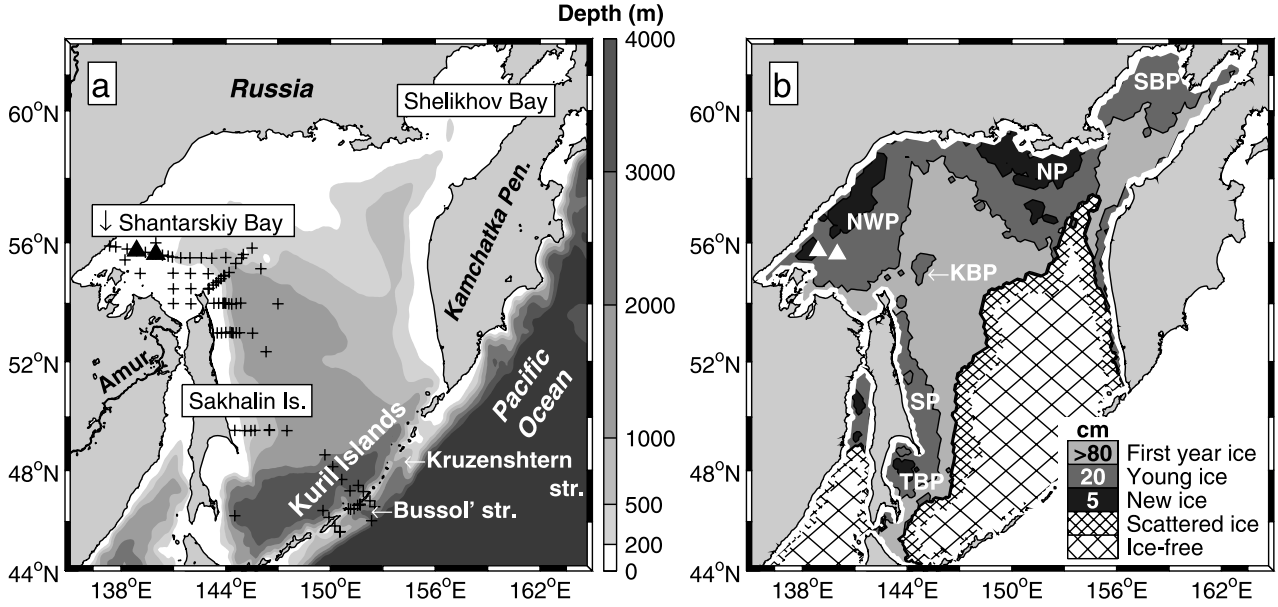

Figure 1. Okhotsk Sea. (a) The topographic map shows station positions of the September 1999 hydrographic survey (pluses) and bottom mooring locations (triangles). Most of the stations were repeated during the June 2000 survey. (b) Ice distribution on 1 February 2000 shows the persistent polynyas: Shelikhov Bay (SBP), northern (NP), northwestern (NWP), Kashevarov Bank (KBP), Sakhalin (SP), and Terpeniya Bay (TBP). Ice classification is based on National Snow and Ice Data Center SSM/I brightness temperatures. White triangles show the bottom mooring positions.

study. An overview of the water mass structure on the shelf in autumn and spring based on the two hydrographic surveys is given in section 3. The ice cover is discussed in section 4. Evolution of bottom water properties and velocity fields in the course of the winter is described in sections 5 and 6. Section 7 summarizes the main findings of the study and their implications. An accompanying paper [*Shcherbina et al.*, 2004] combines the direct mooring observations with the meteorological reanalysis and satellite ice-cover data to estimate the DSW formation and export rates.

2. Data

[7] In situ observation of the processes inside the NWP during wintertime convection was made using an array of four bottom moorings deployed on the shelf of Shantarskiy Bay (Figure 1) in September 1999, two of which were successfully recovered in June 2000. The two surviving moorings were located at (55°45′N, 138°54′E) and (55°39′N, 140°00′E) in 109 and 144 m of water correspondingly, and will hereinafter be referred to as the "inshore" (western, shallower) and the "offshore" (eastern, deeper) moorings.

[8] Each mooring was equipped with a Seabird Seacat CTD and an upward looking 300-kHz broadband RD Instruments acoustic Doppler current profiler (ADCP). Pressure, salinity, temperature, and oxygen concentration were recorded with a 15-min sampling interval. Both CTDs were calibrated before and after the deployment. Observed instrument drift was insignificant (of order of 2×10^{-4} °C yr^{-1} and 1×10^{-2} psu yr^{-1} for temperature and salinity, correspondingly). In the final data calibration, the drifts were linearly distributed throughout the deployment period. The ADCPs provided velocity data with 4-m vertical and 16-min temporal resolution. The first usable bin was located 14.1 m above the bottom. Owing to the lack of scatterers in the water column throughout the year and especially in winter, only a 20–50% data return rate was observed in near-surface (maximum range) layers. The range of 95% data return rate was at 50 and 60 m above the bottom at the inshore and offshore moorings, respectively.

[9] To establish the larger-scale context of the experiment, two hydrographic surveys were performed in September 1999 and June 2000. The surveys consisted of 86 and 111 stations correspondingly (Figure 1) covering the northwestern and Sakhalin shelves as well as Bussol' Strait. They included CTD sampling of pressure, temperature, and salinity and rosette sampling of salinity, oxygen, and nutrients (silicate, nitrate, phosphate, nitrite, ammonium). A lowered ADCP was also mounted on the rosette frame.

3. Water Properties of the Northwestern Okhotsk Sea

[10] The dominating topographic feature of the northwestern Okhotsk Sea is a relatively broad (200–300 km) shelf with typical depth of 100–200 m (Figure 1a). This shelf is characterized by strong tides and accounts for a significant portion of global tidal energy dissipation [*Kowalik and Polyakov*, 1998; *Egbert and Ray*, 2000] (see also section 6.3). The mean cyclonic wind-driven circulation supplies this region with water of North Pacific origin, imported through the northern Kuril straits. Significant water mass modification occurs on the northern shelves due to brine rejection in coastal polynyas in winter, freshwater

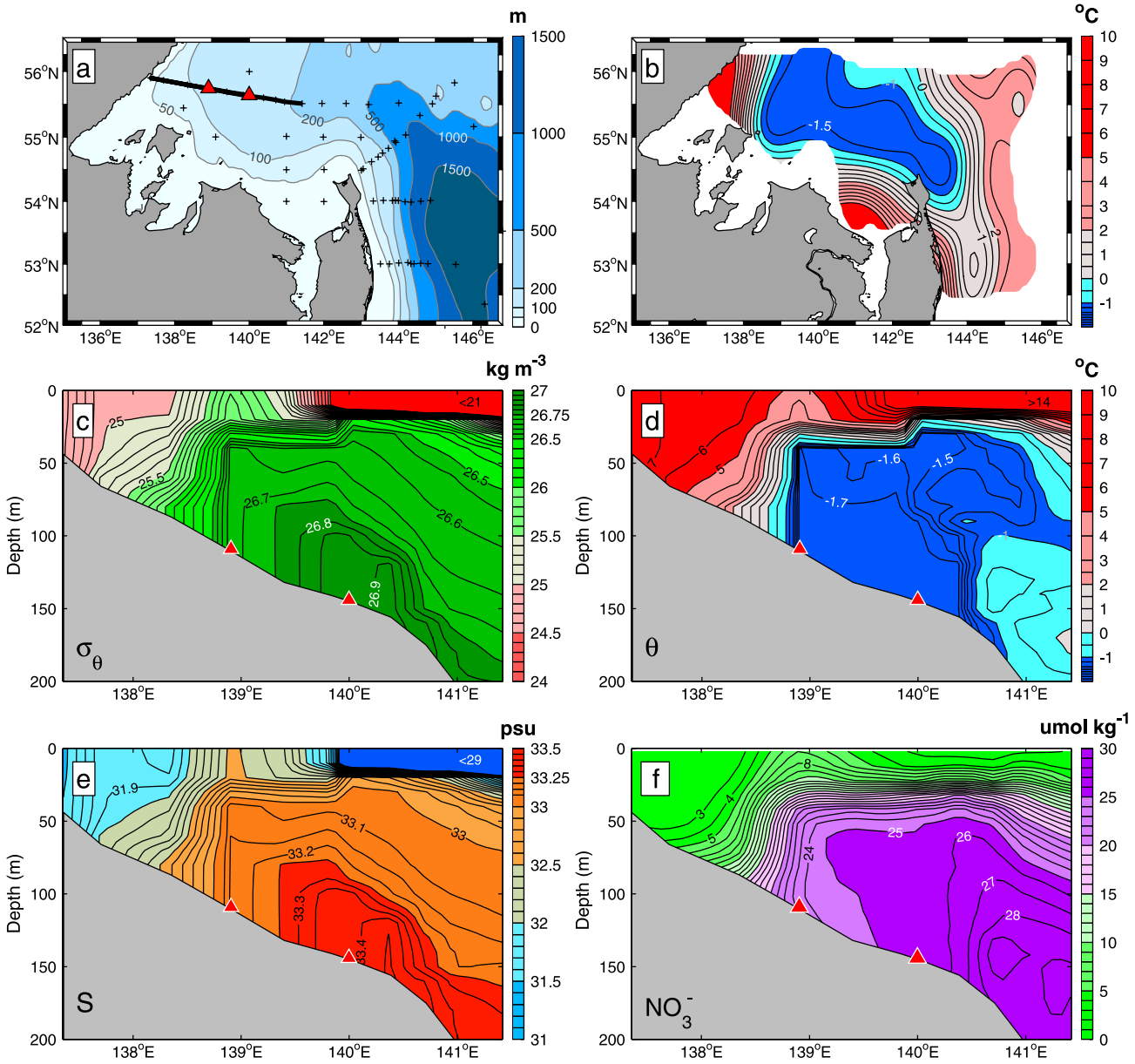

Figure 2. Hydrography of the northwestern shelf in September 1999. (a) Topographic map showing station positions (crosses), bottom mooring locations (triangles), and cross-shelf section location (thick line). (b) Distribution of bottom potential temperature. Vertical cross-shelf sections of (c) potential density, (d) potential temperature, (e) salinity, and (f) nitrate concentration. Section location is marked by thick line in Figure 2a.

input from ice melt and river runoff in summer, and tidal and convective mixing. As a result, several distinct transitional water masses are commonly observed in this region [*Moroshkin*, 1968], as described in the following sections based on our observations.

3.1. Dense Shelf Water

[11] DSW is formed on the northern shelves of the basin each winter [*Kitani*, 1973; *Gladyshev et al.*, 2003]. Both surveys showed the presence of DSW as a bottom temperature minimum on the shelf north of Sakhalin, extending into the East Sakhalin Current (Figure 2). Even in autumn (Figures 2a and 2c), the bottom potential temperature was within 0.1°C of freezing. The DSW layer was about 30 m thick and was located along the bottom between 100 and 160 m depth with maximum density of 26.93 σ_θ observed at 150 m (Figure 2b).

[12] Property distributions observed in June 2000 (not shown) were qualitatively the same as in September 1999. However, the layer of dense water reached 50 m thickness and extended farther inshore. The maximum density was lower (26.81 σ_θ) and was found near the bottom at a shallower (140 m) depth. This difference is the manifestation of interannual variability of the dense water production, which is strongly dependent on winter weather and ice conditions. The winter of 1999–2000 was considerably

milder than the previous one, with the mean February 2000 temperature in the northwestern polynya more than 6°C higher than in 1999. Consequently, the dense water production was weaker, and the maximum density observed during the winter of our experiment (26.92 σ_θ, see section 5.1) was lower than during the previous winter.

3.2. Surface and Nearshore Waters

[13] The offshore stratification during both surveys was capped by a warm and fresh surface mixed layer with densities as low as 21 σ_θ (Figure 2b). In a narrow nearshore band (less than 100 m deep), this layer extended to the bottom likely due to vigorous tidal mixing. Summer sea ice melt likely provides most of the fresh water to this water mass. Even though the freshwater river discharge into the Sea of Okhotsk is quite high (463 km^3 per year), 68% of it comes from the Amur River [*Aota and Ishikawa*, 1991], whose estuary is located farther south (53°N) and likely has little influence on the northwestern shelf. The annual precipitation, which exceeds evaporation by 382 km^3 yr^{-1} and has a summer maximum [*Aota and Ishikawa*, 1991], may also take part in the nearshore and surface water freshening. For comparison, sea ice melt can be estimated to yield about 500 km^3 of fresh water over the whole basin upon melting in early summer.

[14] Even though in summer the lateral extent of this nearshore water mass is limited and it is separated from the DSW by a tidal mixing front (Figure 2b), it likely plays a leading role in the dense water formation during the winter. As will be shown in the next section, this fresh nearshore water was transformed into DSW by brine rejection during the ice formation season.

3.3. Tidal Mixing Front

[15] An important feature of the water property distribution on the northern shelves is the 100-km-wide front separating the mixed nearshore waters (7.6°C, 31.5 psu in September 1999) from the offshore stratified region (−1.72°C, 33.16 psu at the bottom) (Figure 2). The potential density difference along the bottom was approximately 2 kg m^{-3}, implying a baroclinic Rossby deformation radius of order 10 km. The offshore edge of the front was located approximately at the 110- and 90-m isobaths in September 1999 and June 2000, respectively. Both in autumn and in spring the front extended from the bottom to the mixed layer (Figure 2; spring is similar). Additionally, a region of anomalously cold and salty mixed layer water was associated with the top of the front (at approximately 139°E) in autumn (Figures 2d and 2e). This region was also characterized by increased nutrient concentration. (The nitrate distribution is shown in Figure 2f; phosphate and nitrite distributions are similar.) This suggests enhanced exchange between the surface and bottom layers near the front. It is unclear whether this enhancement is due to upwelling or enhanced mixing, or a combination of the two.

[16] The front is likely created by shoaling of the tidal bottom boundary layer. Similar fronts are commonly observed in tidally active shelf regions [*Simpson and Hunter*, 1974; *Simpson*, 1981]. There are also accounts of increased vertical mixing within such fronts [*Ullman et al.*, 2003]. The boundary layer is clearly seen in the density distribution (Figure 2c) as a region of low stratification along the bottom, thickening toward the shore. At approximately 100 m depth the tidal mixing within the layer overcomes the stabilizing effect of the seasonal thermocline and penetrates to the surface, thus creating the front. Inshore of the front the tidal mixed layer spans the whole water column, eliminating much of the vertical stratification.

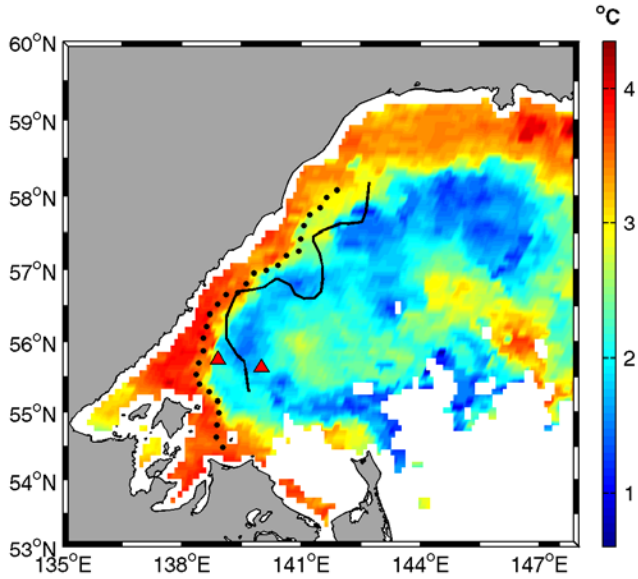

Figure 3. Sea surface temperature on 3 November 1999. Front locations derived from the similar images taken on 19 October (dots) and 17 November (black line) are shown. Red triangles mark the mooring positions. Ocean Pathfinder advanced very high resolution radar data were obtained from the NASA Physical Oceanography Distributed Active Archive Center at the Jet Propulsion Laboratory, California Institute of Technology.

[17] In late autumn 1999, the front shifted offshore, as evident from the satellite observations of sea surface temperature (Figure 3). This transition was also registered in properties and velocities in mid-November by the inshore mooring, but not at the offshore mooring (see section 5.1 and Figure 5 in section 5). Apparently, the front stayed between 139°E and 140°E (between the moorings) until it was modified by the new dense water formation. As a result, the initial conditions at the beginning of ice formation and brine rejection at the two moorings were significantly different, which may account for differences in the water mass evolution observed at those sites.

[18] Numerical modeling of tidal mixing fronts [*Simpson*, 1981] suggests that the movement of the front could be caused by the erosion of the shelf stratification due to surface cooling in autumn. Decreased stratification in autumn would facilitate vertical mixing, allowing a thicker boundary layer. As a result, the boundary layer would shoal at a deeper location, leading to the offshore shift of the front.

4. Wintertime Evolution: Ice Cover

[19] Sea ice distribution throughout the winter was observed using the 25-km gridded Special Sensor Microwave Imager (SSM/I) brightness temperature data [*Maslanik and Stroeve*, 2003]. The "thin ice" algorithm [*Cavalieri*, 1994;

Kimura and Wakatsuchi, 1999] was used to determine the ice extent and distinguish between the new, young, and first-year ice fractions. The classification is semi-empirical: The "new" ice fraction generally corresponds to frazil, grease, nilas, pancake ice types; "young" ice fraction corresponds to thin (gray) first-year ice; "first year" ice fraction corresponds to thick (white) or snow-covered first year ice [*Cavalieri*, 1994]. There is no multiyear ice present in the basin.

[20] Freezing of the Okhotsk Sea in the winter of 1999–2000 started in late December (Figure 4). Ice cover was first established in the Shelikhov and Shantarskiy bays and along the coast and then progressed into the middle of the basin. Maximum ice extent was reached in the middle of March, and the ice virtually disappeared by June.

[21] The northwestern polynya (NWP), seen as an area of thinner ice over the northwestern shelf (Figure 4), was active from late January to mid-March. Its counterpart, the northern polynya (NP), persisted until early April. Both polynyas closed briefly on 15 February. Even though the NP had a larger lateral and temporal extent, the ice was generally thinner inside the NWP, resulting in greater heat loss than in the NP [*Shcherbina et al.*, 2004].

5. Wintertime Evolution: Bottom Water Properties

[22] The time series of bottom water properties recorded by the moorings are shown in Figure 5. The records span 9 months of the annual cycle of DSW evolution, including the active brine rejection in winter, preconditioning phase in late autumn, and the summertime period of gradual export of dense water from the shelf region. The following subsections focus on various stages of this cycle, with a summary in section 5.5.

5.1. Brine Rejection

[23] Dense shelf water formation is evident in the bottom salinity, potential temperature, and potential density time series (Figure 5). A salinity increase associated with brine rejection started at the inshore (western) mooring on 20 January 2000, soon after ice cover at the site was established. A near-linear salinity increase continued through 23 February, reaching a maximum salinity of 33.45 psu, for a total of 0.83 psu salinity increase in 35 days. This corresponds to a σ_θ = 0.68 kg m^{-3} potential density increase, reaching a maximum potential density of 26.92 kg m^{-3}. A subsequent short-term salinity burst on 15–17 March produced an absolute maximum salinity of 33.49 psu (26.95 σ_θ).

[24] DSW formation in 1999–2000 was confined to the area shoreward of the deeper, offshore mooring. No significant salinity increase was observed at the offshore mooring, indicating no active brine rejection penetrating to the bottom. This is a major contrast with the inshore mooring, even though the instruments were less than 70 km apart. Instead, a slow, steady salinity increase was observed from 16 January to the end of the record in June, probably due to gradual export of dense water from the polynya.

[25] It is worth noticing that the density difference between the two moorings was close to 0.3 kg m^{-3} both before and after the density increase period, although the signs of this difference were opposite. The Rossby deformation radius corresponding to this difference was approximately 5 km. Additionally, the density increase at the inshore mooring stopped briefly when it reached σ_θ = 26.58, the density observed at the same time at the offshore mooring. It is presently unclear whether these matches are purely coincidental or are a result of the dynamics of the polynya region.

5.2. Preconditioning

[26] The wintertime brine rejection at the inshore mooring was preceded by a sharp 0.5-psu salinity drop and a concurrent 2.5°C temperature increase in mid-November, associated with the transition of the tidal mixing front (see section 3.3) offshore of the mooring site (Figure 5). Even though the temperature returned to near freezing by mid-January, the salinity recovered only insignificantly. As a result, the density of the water present at the inshore mooring when ice formation started (DSW precursor water) was at least 0.25 kg m^{-3} lower than in early November. Taking into account the preceding density decrease in September and October, this water density is 0.43 kg m^{-3} lower than could be inferred from the September survey alone. This result shifts the attention to the fresh, well-mixed inshore water as the source for DSW formation.

5.3. Potential Supercooling

[27] Evidence of surface supercooling was observed during the brine rejection phase at the inshore mooring based on the near-bottom temperature record. The bottom potential temperature stayed 7 × 10^{-3} °C below the surface freezing point (Figure 6) from 24 January to 4 March, with a short break on 17 February. We term this effect "potential supercooling," as the bottom water with the observed temperature and salinity would be supercooled if shifted adiabatically to the surface. Using this term, we explicitly distinguish this effect from in situ supercooling, which was not observed at our moorings.

[28] We assume that this cold water was brought from the surface by convection, probably driven by brine rejection. Additionally, we assume that the water column was well mixed by such convection, so the potential temperature at the bottom was equal to the surface temperature or slightly higher due to the mixing of the convective plumes with warmer surrounding water. Consequently, we conclude that the surface water was supercooled by at least 7 × 10^{-3} °C. No persistent potential supercooling was observed at the offshore mooring.

[29] Surface supercooling of up to 0.1°–0.2°C has been found experimentally to be a characteristic feature if not a necessary condition of frazil ice formation [*Ushio and Wakatsuchi*, 1993]. Episodical supercooling events associated with frazil ice formation have also been observed by *Drucker et al.* [2003] at 30–40 m below the surface. Unlike Drucker et al.'s observations, the potential temperatures observed during our experiment were below the surface freezing point, but above the in situ freezing point, so ice formation was not possible at the depth of our measurements. (The bottom temperatures would be consistent with ice formation to a maximum depth of 10 m, assuming no admixing of warmer waters during convection.) Our observation of potential supercooling serves as an important

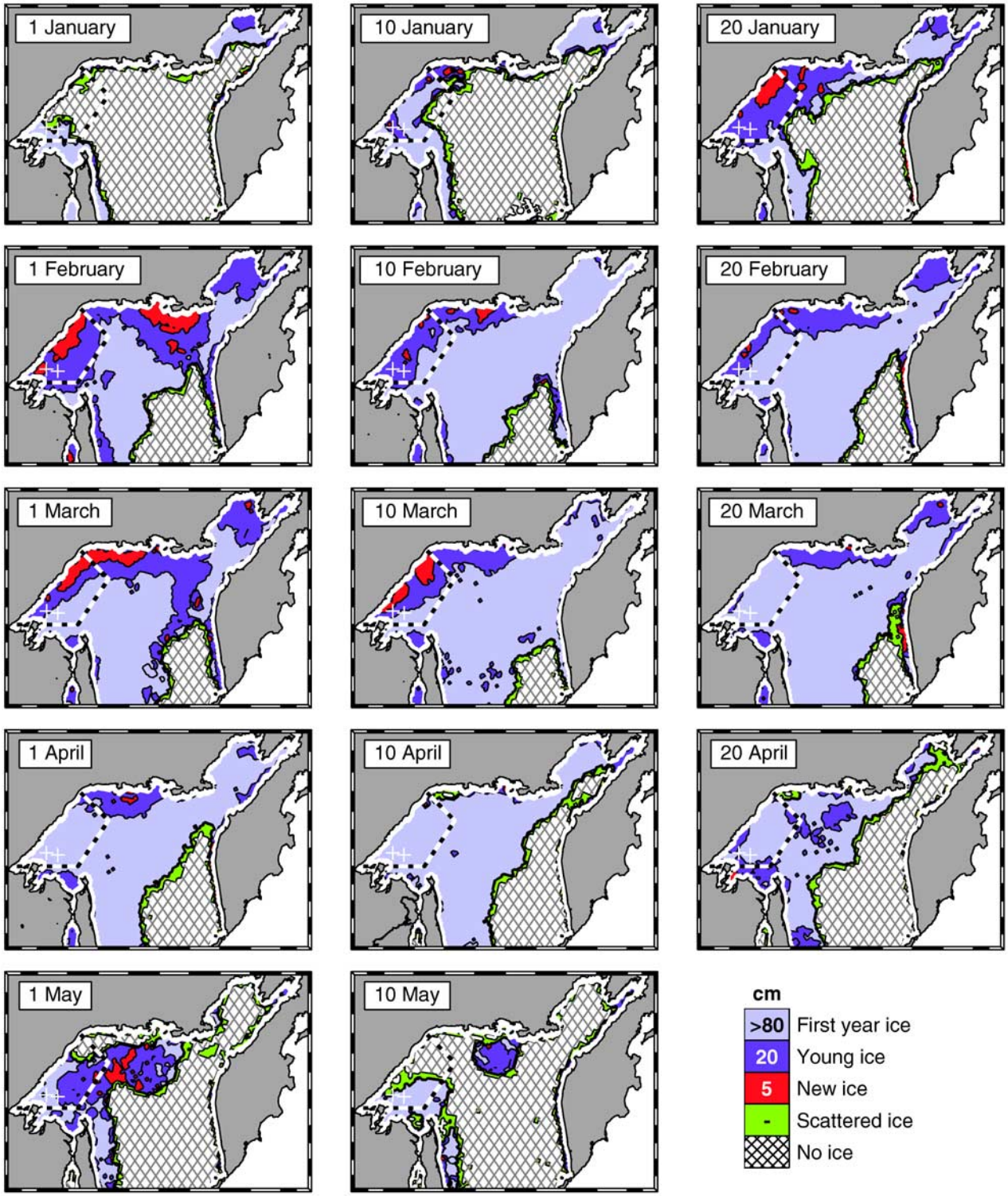

Figure 4. Evolution of ice cover in the northern Okhotsk Sea in early 2000. Ice classification is based on National Snow and Ice Data Center SSM/I brightness temperatures. Typical ice thickness (in centimeters) of the ice types is marked on the legend. Northwestern polynya region boundary is marked by dashed line. White crosses mark the mooring locations.

indicator of active near-surface frazil ice formation at the mooring site. This is further supported by the general coincidence of supercooling events with the periods of thinner ice cover above the mooring (Figure 6b).

[30] It is worth noticing that the potential temperature at the inshore mooring dropped below the surface freezing point simultaneously with the start of the density increase, but then persisted for approximately 10 days after the

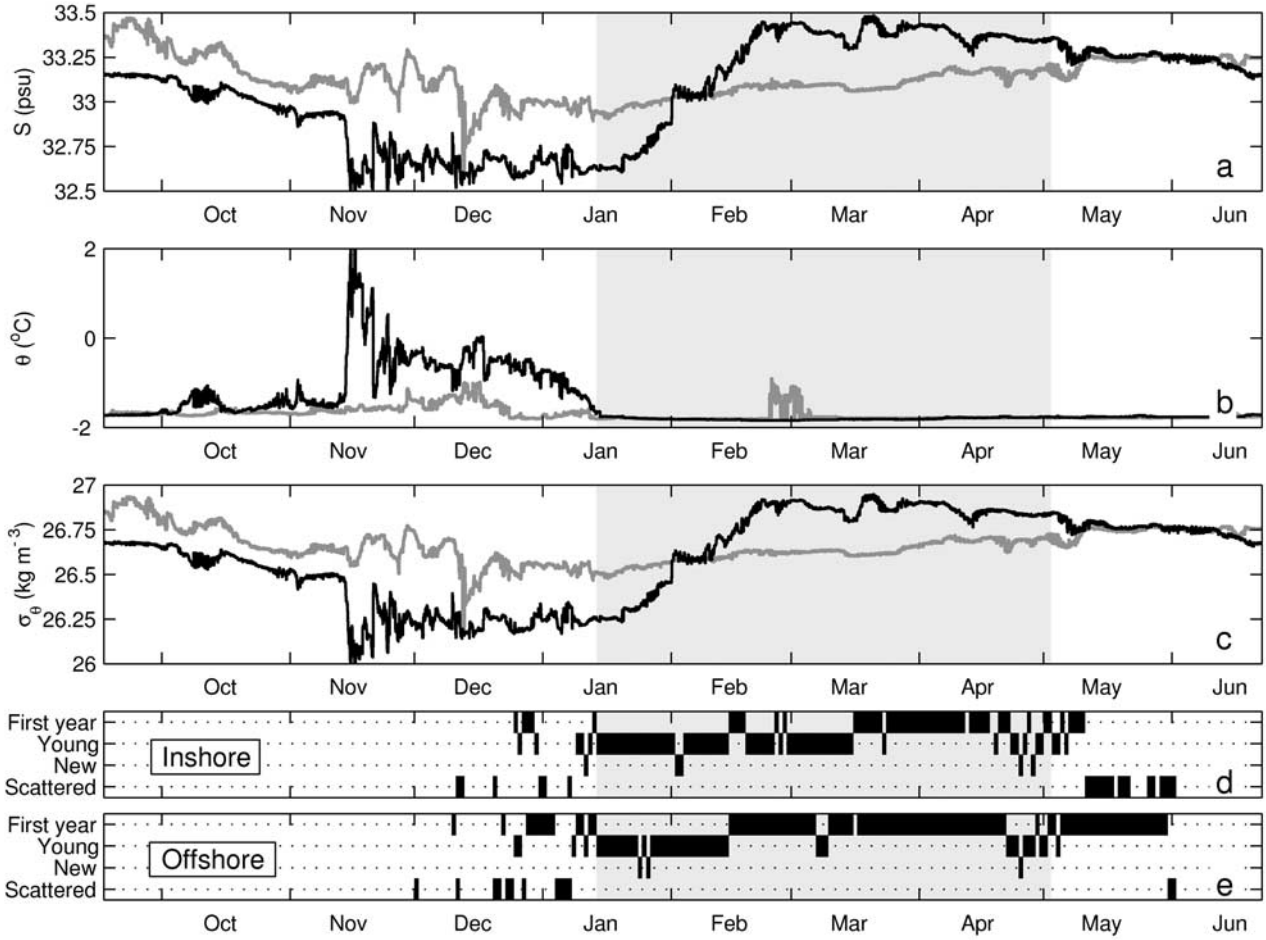

Figure 5. Bottom water properties at the moorings. (a) Salinity, (b) potential temperature, and (c) potential density on the inshore (black line) and offshore (shaded line) bottom moorings. Shading represents the ice-covered period at the inshore mooring (based on ADCP surface reflection intensity). Ice classification at the (d) inshore and (e) offshore moorings based on SSM/I brightness temperatures is also shown. Black bars indicate presence of a given ice type. Ice types are the same as in Figure 4.

density increase stopped. This suggests that the brine rejection and DSW formation continued at least through the beginning of March, but its last phase was not accompanied by densification.

5.4. Passage of a Warm Eddy Through the Offshore Mooring Site

[31] An abrupt short-term temperature increase occurred at the eastern (offshore) mooring between 25 February and 6 March (Figure 5). Potential temperature of up to $-0.9°C$ was observed during that period, which is an absolute maximum over the whole 9-month record at this site. The increase consisted of a series of bursts, between which the temperature recovered to its near-freezing values. The bursts were quasiperiodic with intervals of 12 ± 2 hours between them, suggesting the tidal nature of the observed fluctuations. The temperature fluctuations were well compensated in their effect on density with corresponding salinity changes (Figure 7b). On the basis of the autumn isopycnal distribution of temperature (not shown), such warm water likely originated from at least 60 km east of the mooring site. The warming was also accompanied by clockwise rotation of the flow at this offshore mooring, which led to a period of onshore (northwestward) flow (Figure 9 in section 6). This likely indicates the passage of a warm-core eddy through the site of the mooring. On the basis of the velocity and temperature observations, the eddy size was of an order of 10 km with characteristic rotation velocity of about 5 cm s^{-1}. The observed tidal pulsation of temperature was likely due to the strong near-bottom stratification within the eddy.

5.5. DSW Evolution Cycle

[32] Overall, the evolution of bottom water properties in the polynya region followed an annual cycle (Figure 7a), consisting of several distinct phases.

[33] 1. During the first (winter) phase (late January to late February) the salinity rapidly increased due to brine rejection. The bottom potential temperature stayed slightly below the surface freezing point, suggesting that the surface water was supercooled (section 5.3).

[34] 2. The linear density increase terminated abruptly on 23 February, even though the polynya was still open and the active ice formation and brine rejection continued (as

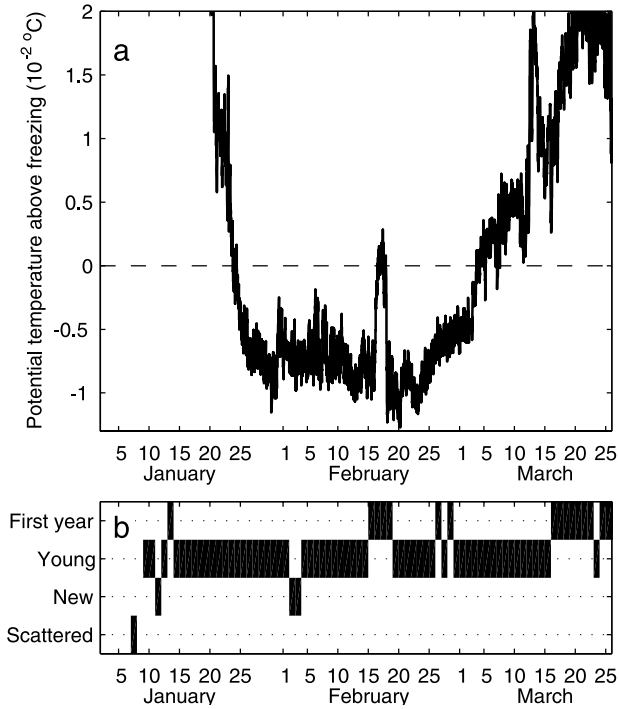

Figure 6. Potential supercooling at the inshore mooring. (a) Difference between the bottom potential temperature and the freezing point at the bottom salinity and atmospheric pressure is plotted. (b) Ice classification based on SSM/I brightness temperature. Black bars indicate presence of a given ice type. Ice types are the same as in Figure 4.

evident from ice observations and potential supercooling). This is further supported by the analysis of heat balance over the mooring sites (Figure 8), which found no significant changes in the surface heat loss at the time of density increase termination. (Details of heat flux calculations are given in the accompanying paper [*Shcherbina et al.*, 2004].) Consequently, during the late stages of DSW formation, the salt influx would have been balanced by enhanced export of excess salt from the polynya region.

[35] Similar abrupt termination of density increase under continuing buoyancy forcing has been modeled numerically [*Gawarkiewicz and Chapman*, 1995]. Their model predicts initial linear increase of density within the polynya region, leading to the formation of a sharp density front at its offshore boundary. Geostrophic adjustment of the front incites counter-rotating rim currents in the bottom and surface layers. Intrinsic instability of this system results in meandering and eventual formation of baroclinic eddies that transport brine-enriched water away from the polynya region while replacing it with fresher water from offshore. Enhanced cross-shelf exchange that results from this process balances salt flux driven by brine rejection in the polynya, leading to a dynamical equilibrium. The velocity record analyzed in the following section provides indirect evidence of such enhanced eddy activity at the inshore mooring between February and May 2000.

[36] 3. In spring and summer, salinity at the inshore mooring steadily decreased, suggesting gradual replacement of DSW with fresher water from the northern shelves. Such "flushing" would continue each year until late autumn: The same salinity decrease can be seen through autumn at the beginning of the record. The offshore transition of the tidal mixing front in late autumn brought a significant salinity drop and temperature increase to the inshore mooring. Early winter cooling then brought the temperature to the freezing point, concluding the cycle.

[37] The exact path of the DSW cycle in temperature-salinity space must depend on the particular weather conditions for each given year. Projecting the spring 2000 salinity decrease to the autumn of 2000 would result

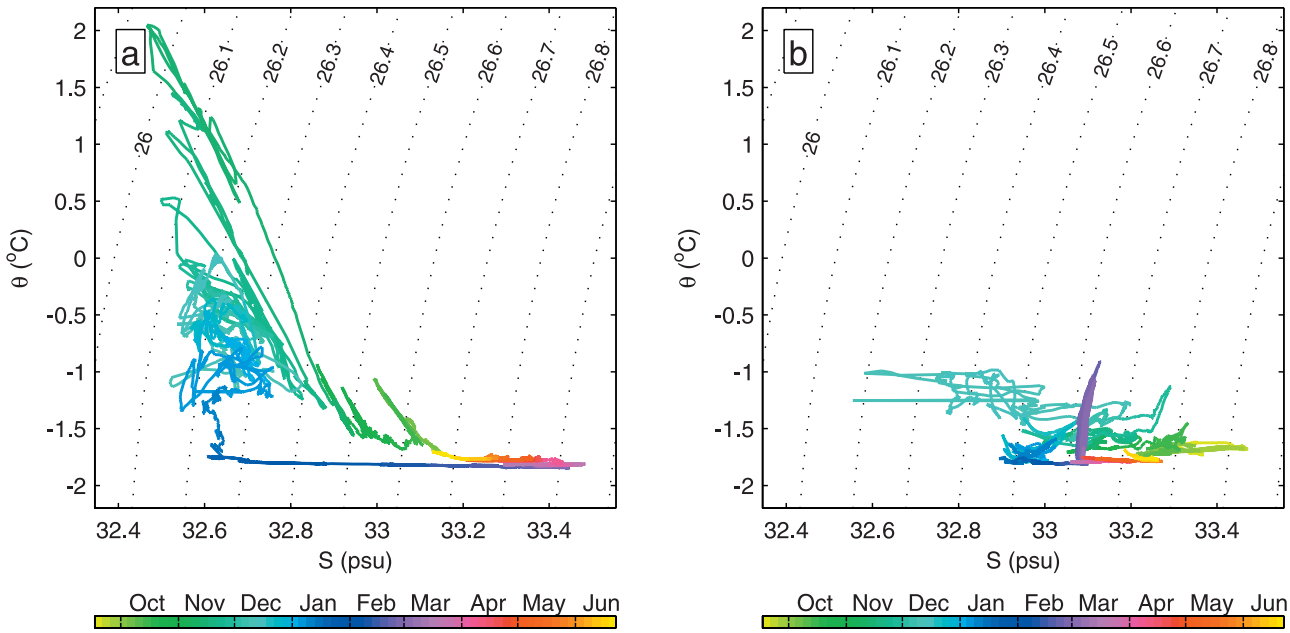

Figure 7. Scatterplots of bottom water properties at (a) inshore mooring and (b) offshore moorings, color-coded with time. Dashed lines are isopycnal (σ_θ = const) contours (labeled in kg m^{-3}).

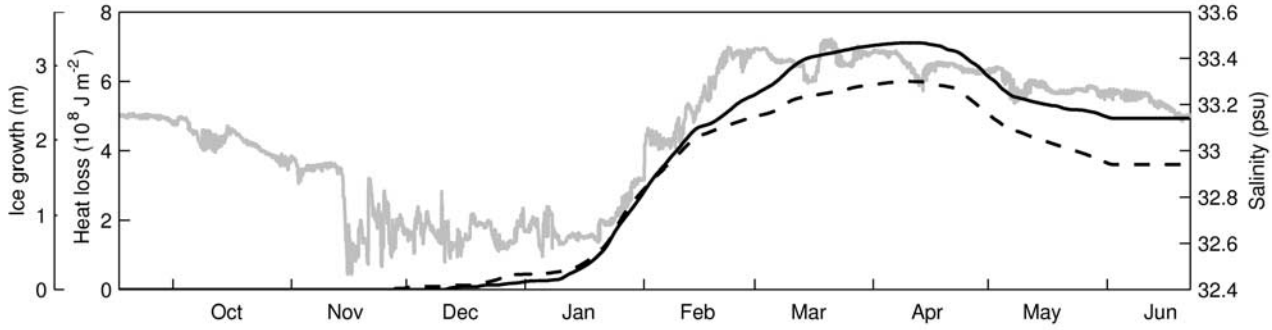

Figure 8. Cumulative heat loss through the ice above the inshore (solid black line) and offshore (dashed black line) mooring site. The leftmost scale shows the ice growth equivalent to this heat loss. Salinity at the inshore mooring (shaded line) is shown for reference. The estimates of heat fluxes and ice classification are based upon ECMWF reanalysis meteorology and National Snow and Ice Data Center ice data, respectively.

in lower salinity than was observed in autumn of 1999. The salinity of 33.15 psu observed at the inshore mooring in September 1999 was actually reached again by June 2000. This is a manifestation of the interannual variability of DSW properties and production rates. The winter of the experiment (1999–2000) was considerably milder than the previous one, with the mean February 2000 temperature in the region of northwestern polynya over 6°C higher than in 1999 (based on European Centre for Medium-Range Weather Forecasts (ECMWF) data). Consequently, the DSW production was likely weaker and DSW properties were less extreme in early 2000 than during the previous winter.

[38] The seasonal cycle of bottom water properties observed at the offshore mooring was radically different, even though the moorings were less than 70 km apart and both were located within the northwestern polynya. The period of thin ice cover (young and new ice types) over the offshore mooring was considerably shorter than over the inshore one. However, the cumulative heat loss over these sites was almost identical until mid-February and differed by only 20% by the end of the season (Figure 8). Despite that, both the preconditioning and brine rejection phases were missing from the offshore mooring record, and no DSW formation was observed there. The reason for the difference between the two sites is not clear, but may be due to the location of the winter tidal shelf front, and its feedback, through mixing, on the location of the thinnest ice in the NPW.

6. Wintertime Evolution: Velocity Field

[39] The velocity time series at the two moorings (Figure 9) were well correlated with each other. Their mean values were nearly equal: 6.35 cm s^{-1} at the inshore mooring and 6.40 cm s^{-1} at the offshore one. The mean flow was directed southwest approximately along isobaths. (A detailed investigation of the relation of the flow to the local topography is impossible due to lack of sufficient information about the latter.) This flow direction is consistent with the general cyclonic circulation in the Okhotsk Sea [*Ohshima et al.*, 2004]. The flow exhibited significant

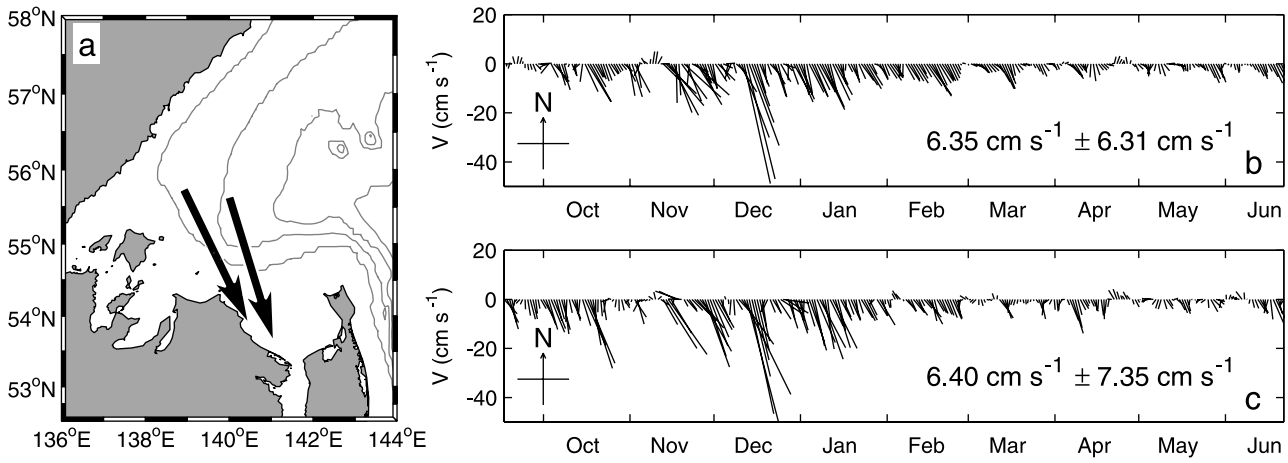

Figure 9. (a) Mean flow and the velocity vector time series at (b) inshore and (c) offshore mooring (vertical mean, 48-hour Blackman filter low pass). Both direction and amplitude are shown (north is up). Absolute mean and standard deviation are shown for each time series.

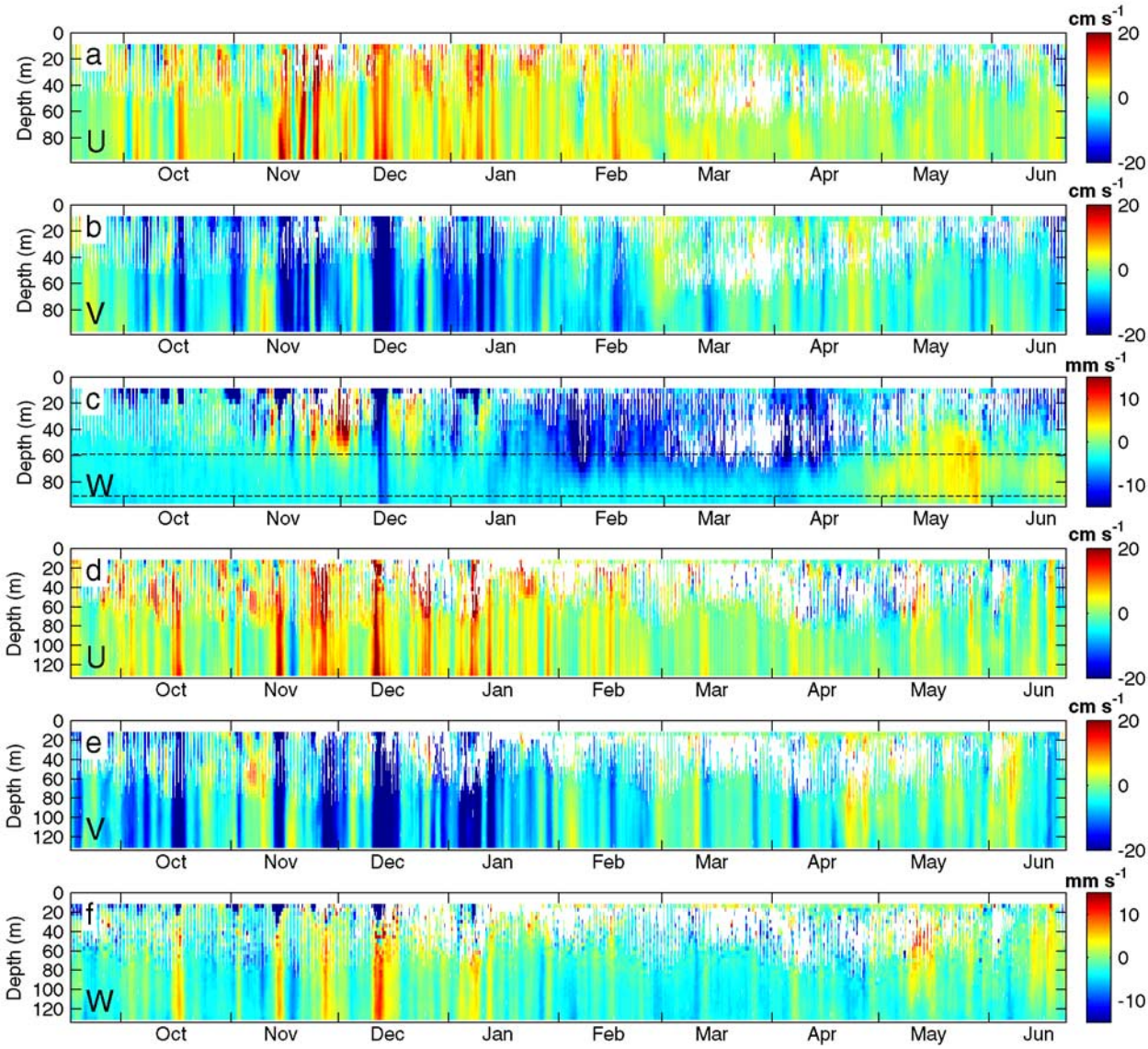

Figure 10. ADCP velocity record at (a–c) inshore and (d–f) offshore moorings. Eastward (Figures 10a and 10d), northward (Figures 10b and 10e), and upward (Figures 10c and 10f) velocities are shown. White areas indicate missing data. Data were low-passed with 48-hour Blackman filter. Bi-monthly histograms of vertical velocity distribution at the horizons marked by dashed line in Figure 10c are shown in Figure 11. Note different scales for horizontal and vertical velocity plots.

seasonal variations (section 6.1) and was generally much weaker than the barotropic tides. The tidal amplitudes were an order of magnitude larger than the long-period variability, so the tidal and subtidal flow variability will be discussed separately in section 6.3.

6.1. Subtidal Horizontal Flow Variability

[40] Low-frequency (subtidal) horizontal velocities measured at both moorings were fairly barotropic throughout the deployment period (Figure 10). The records show a general increase of southward flow between October and January, with weaker flow during the ice-covered period that followed (Figure 9b). Such variation is consistent with the seasonal changes of the basin circulation in response to the large-scale wind-forcing variations [*Ohshima et al.*, 2004]. The strongest flow (over 50 cm s^{-1} on both stations) was registered during the storm of 12 December 1999 when the wind reached its maximum over the observation period (19 m s^{-1} based on ECMWF meteorological reanalysis).

6.2. Vertical Velocity Variability

[41] Negative mean vertical velocity was measured at both moorings: -3.8 mm s^{-1} (inshore) and -1.7 mm s^{-1} (offshore). These values are too large and too depth independent to be explained by the effects of the bottom slope (even though the exact local slopes are unknown due to poorly resolved topography) and are likely a measurement artifact. Similar negative bias in the vertical velocity ADCP record has been previously reported by *Schott et al.* [1993].

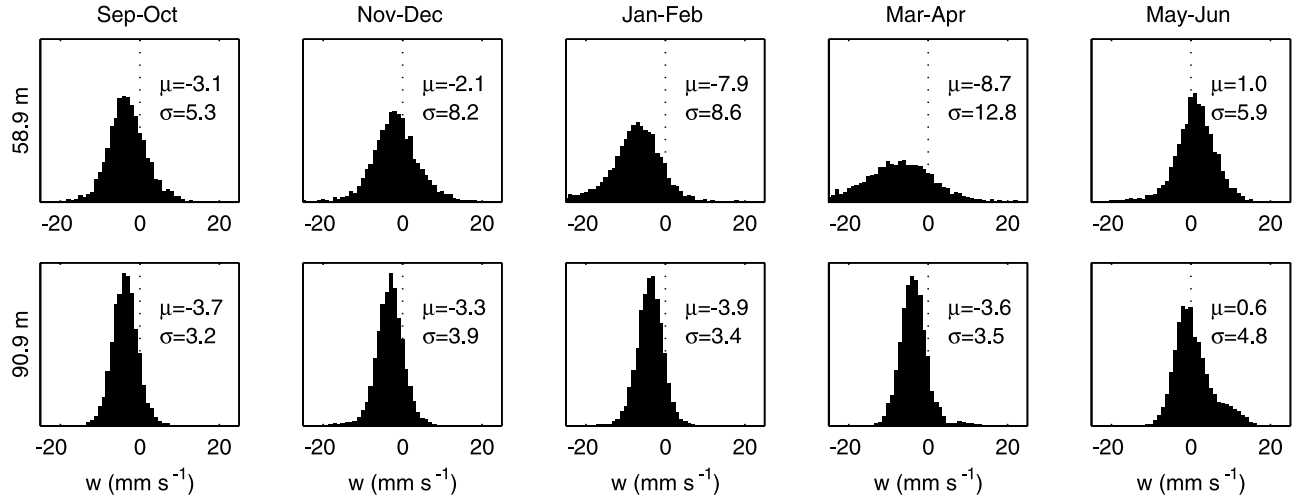

Figure 11. Bi-monthly histograms of unfiltered vertical velocity at the inshore mooring at 59 m (top row) and 91 m (bottom row) depth levels (shown by dashed lines in Figure 10c). Columns represent 2-month periods as marked at the top. Mean (μ) and standard deviation (σ) values are given for each distribution (in mm s^{-1}).

The bias is assumed to be time independent, so the seasonal variation of vertical flow with respect to the mean can still be investigated.

[42] An intriguing feature of the vertical velocity recorded at the inshore mooring is the enhancement of downward flow in the upper 70 m of the water column between mid-January and late April, followed by an upward flow anomaly near the bottom in May and June (Figure 10c). The period of anomalous downward flow coincides remarkably well with the presence of ice cover over the mooring, as determined by the intensity of ADCP surface echoes (Figure 5). The standard deviation of vertical velocity was also higher during this period (Figure 11), and the distribution was noticeably skewed toward downward flow. Such vertical velocity behavior is similar to that observed during deep convection events in the Greenland Sea [*Schott et al.*, 1993] and might indicate the presence of convective cells under the ice. Numerical models predict anisotropy of the brine-driven convective cells leading to the downward velocities being several times larger than the upward ones [*Kampf and Backhaus*, 1998]. Such asymmetry would explain both the skewness and the negative mean of the velocity distribution. However, the model also predicts that the scale of downward plumes would be considerably smaller than both the distance between them and the surface spreading of ADCP beams. Consequently, the plume observation is expected to be much more intermittent than the observed persistent anomalous downward flow. On the other hand, the downward flow anomaly at the offshore mooring during the ice-covered period was much weaker (Figure 10f). As evident from the bottom water evolution (section 5.1), active brine rejection was observed only at the inshore mooring. Consequently, it is tempting to suggest that the observation of downward flow is associated with brine rejection and DSW formation. A direct connection, however, cannot be established with this data set.

[43] An upward flow anomaly was observed in May at the inshore mooring and, to a much smaller extent, at the offshore location (Figure 10). The exact nature of this shift is also unknown. Vertical diurnal migration of zooplankton can provide a partial explanation for the skewness of the vertical velocity distribution toward positive values (most prominent in the near-bottom layers, Figure 11). Such migration, resulting in apparent daily spikes of upward flow, is a known artifact in ADCP velocity measurements [*Schott and Johns*, 1987; *Wilson and Firing*, 1992]. Vigorous migration that is also seen in the ADCP echo strength signal (not shown) resumed right after the disappearance of ice cover in early May and caused the observed vertical velocity distribution skewness. The plankton migration hypothesis, however, explains neither the shift of the whole vertical velocity distribution toward positive values in May (Figure 11) nor the virtual absence of such a shift at the other mooring. It also does not negate the observations of the anomalous downward flow during the ice-covered period. Even though the spring upward flow anomaly may have shifted the long-term vertical velocity average, thus increasing the apparent magnitude of the wintertime downward flow anomaly, the latter can be also traced with respect to the late-autumn flow (Figure 10 and Figure 11).

6.3. Barotropic and Baroclinic Tides

[44] The tidal signal at both moorings was much stronger than the mean flow, with amplitudes reaching 50 cm s^{-1}. The major tidal component was M2 with amplitudes of approximately 29 cm s^{-1} at the inshore mooring and 21 cm s^{-1} at the offshore one. The second largest component was S2, with amplitudes of 10 and 7 cm s^{-1}, correspondingly. All components exhibited strong elliptical polarization (ratio of the major to minor axis of about 6), with major axes nearly perpendicular to the isobaths (Figure 12).

[45] Tidal flow was predominantly barotropic with a typical mean vertical shear of about 3×10^{-3} s^{-1}. However, several bursts of high shear occurred at the inshore mooring in the second half of the record. The peaks in the

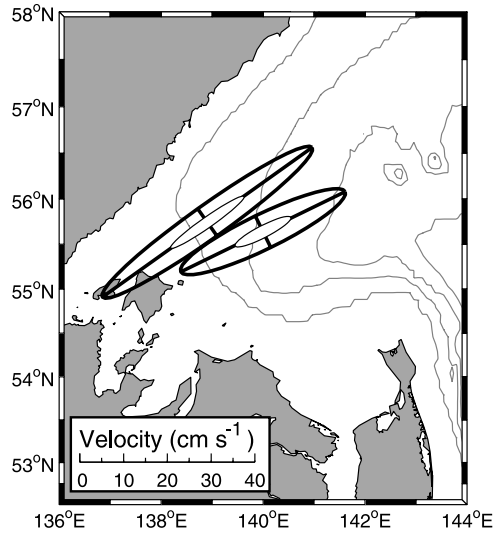

Figure 12. Mean current ellipses for the M_2 (outer ellipse) and S_2 (inner white ellipse) tide.

root mean square vertical shear (Figure 13) coincided remarkably well with prominent disturbances in the density trend. The most energetic event (19–27 February) was associated with the termination of the linear density increase associated with brine rejection in the polynya. (The shear intensification and density drop in mid-November were due to the transition of a tidal mixing front through the mooring site and should be analyzed separately from the winter events.) Several weaker events also occurred later, at quasi-regular intervals of 23–25 days. High shear events exhibited little correlation with the tidal cycle: While the first (24 February) and the last (6 May) of them roughly coincided with spring barotropic tides, the other two occurred closer to the neaps.

[46] Investigation of the temporal frequency structure of vertical shear record (Figure 14) shows that the shear variance peaks were caused by intensification of the semi-diurnal internal tide component. Shear intensification was most prominent in the 30- to 40-m-thick near-bottom layer (Figure 15). Vertical propagation of the vertical shear maximum can be clearly seen during the two strongest events (shown in detail in Figure 15), although the direction of such propagation was different. Such internal tide amplification is likely due to the instigation of vertical stratification associated with the baroclinic instability of the polynya rim current. Series of baroclinic eddies that appear at the later stages of adjustment of density anomaly under a polynya [*Gawarkiewicz and Chapman*, 1995] can create sharp stratified layers, which may allow internal tide generation. Vertical propagation and temporal intermittency of patches of high shear likely reflect the corresponding changes of the high-stratification regions.

[47] No wintertime internal tide intensification events were observed at the offshore mooring (Figure 13b). On the contrary, typical shears at that site during January to March were half as large as during the rest of the record. Only slight shear intensification was associated with the warm eddy passing the mooring in the end of February (see section 5.4). This relatively "quiet" shear field at the offshore mooring yet again supports the conclusion that the two moorings were situated in radically different dynamical regimes, and that only the inshore mooring recorded actual DSW formation.

7. Summary

[48] Dense shelf water formation on the northwestern shelf of the Okhotsk Sea was observed directly for the first time using wintertime bottom moorings. The relatively warm, fresh, well-homogenized water inshore of the shifting tidal mixing front was shown to be the precursor of DSW. This result calls for the reconsideration of DSW formation rate estimates, which have been based on inadequate assumptions resulting from the lack of in situ wintertime data [*Martin et al.*, 1998]. Formation rate estimates using our moored data and findings regarding the precursor DSW are given in the accompanying paper [*Shcherbina et al.*, 2004].

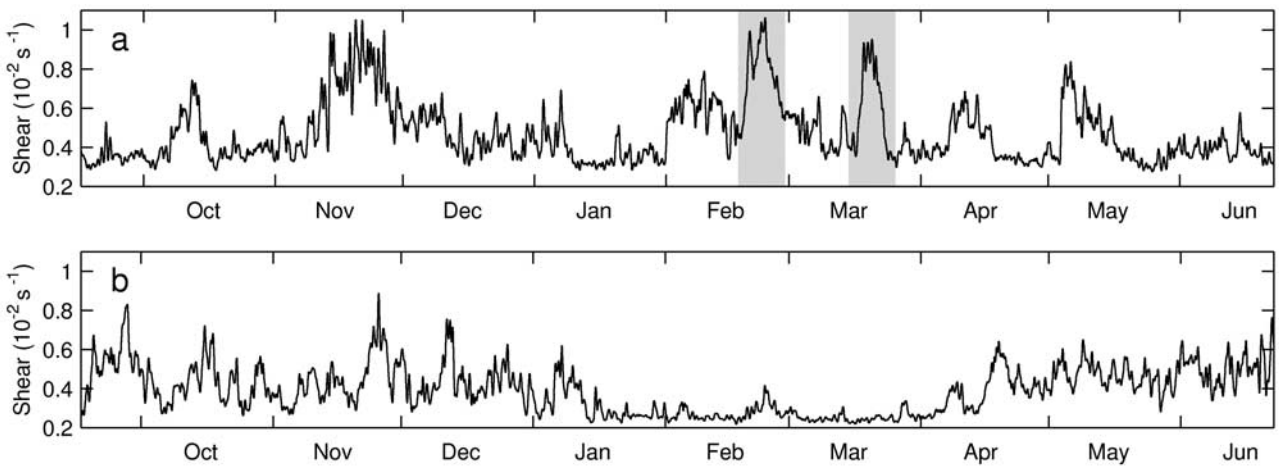

Figure 13. Root mean square vertical shear at (a) inshore and (b) offshore moorings, averaged within 50 m off the bottom and low passed with 24-hour Blackman filter. Details of shaded events are shown in Figure 15. The 95% confidence limits are within 10% of the plotted values.

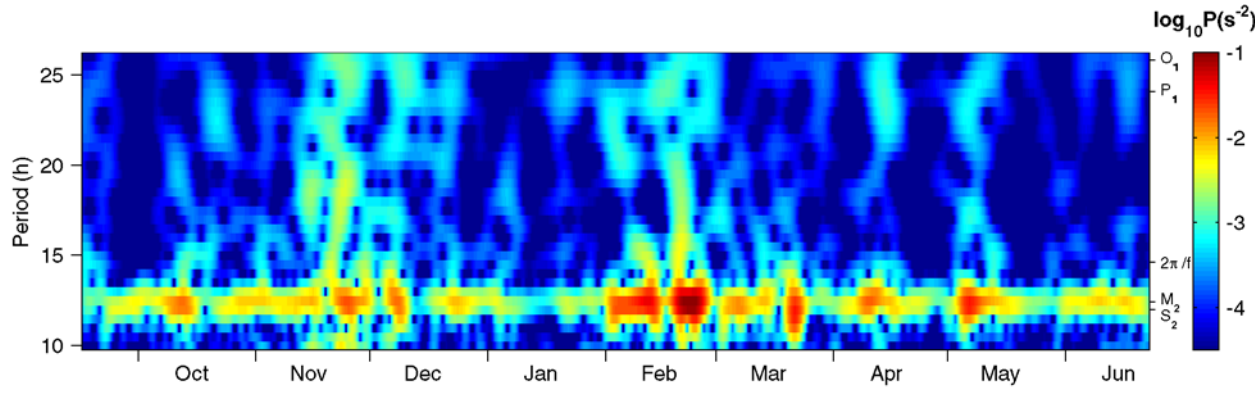

Figure 14. Distribution of vertical shear variance as a function of time and period (clockwise-rotating). Data from 40 m off the bottom at the inshore mooring are shown. Periods of major tidal constituents as well as the inertial period ($2\pi/f$) are marked on the right. Rotary wavelet transform with Morlet wavelet of order $c = 20$ was used.

The nearly linear potential density increase associated with brine rejection continued for over a month in January–February 2000, reaching 26.92 kg m^{-3} (0.68 kg m^{-3} density increase).

[49] The density increase terminated abruptly on 23 February 2000, while the ice formation continued for several more weeks based on the observed potential supercooling and heat flux analysis. The assumed continuing salt flux was likely balanced by the enhanced offshore exchange driven by baroclinic instability at the edge of the forcing region. In the present study, indirect evidence for the presence of baroclinic eddies transporting the density anomaly offshore was provided by periodic intensification of near-bottom internal tides. It is suggested that such intensification indicates periods of high stratification within the eddies. This is further supported by numerical simulations of the process of internal tide generation accompanying the dense water formation (A. Shcherbina, manuscript in preparation, 2004).

[50] In contrast with observations at the inshore (western) mooring, neither the density increase nor the baroclinic tide intensification was found at the offshore (eastern) mooring. These suggest that no DSW formation occurred at the offshore mooring site that winter, or at least that the DSW formed never penetrated to the bottom. Instead, the bottom water density increased slowly, likely due to gradual mixing with the dense water inside the polynya and advection from upstream. This is surprising, since both moorings were located within the active heat loss area of the northwestern polynya, and the density at the shallower inshore mooring was higher that at the offshore one. The mechanisms that set the offshore boundary of newly formed DSW between the two moorings need to be further investigated. In particular, the role of the final position of the tidal mixing front may prove to be important, as the structure of vertical mixing and amount of preconditioning are radically different on either side of it.

[51] The findings of this study emphasize the need for including local shelf dynamics in addition to the external buoyancy forcing when estimating the dense shelf water formation rates. The first step toward this goal, utilizing the information of the observed variability of the advection field, is described in the accompanying paper [*Shcherbina et al.*, 2004].

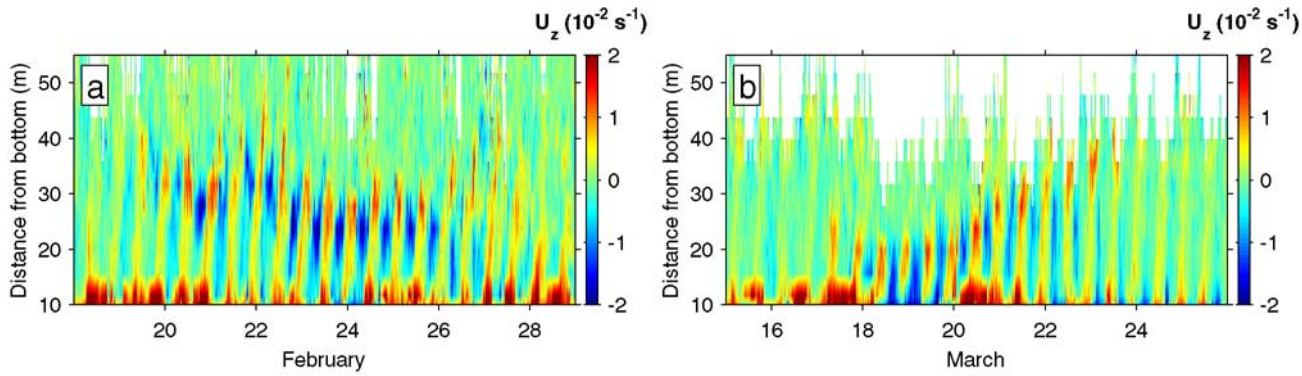

Figure 15. Vertical shear at the inshore mooring during the internal tide intensification events: (a) 18–29 February 2000 and (b) 15–26 March 2000 (periods of these events are shaded in Figure 13). Zonal component of the shear is shown (meridional is similar but offset by $^1/_4$ of the period).

[52] **Acknowledgments.** This work was supported through the National Science Foundation grant OCE-9811958 and by Hokkaido University (ship support). Technical support was provided by the Oceanographic Data Facility and the Instrument Development Group at Scripps Institution of Oceanography (SIO), and by the captain and crew of the R/V *Professor Khromov.*

References

Alfultis, M. A., and S. Martin (1987), Satellite passive microwave studies of the Sea of Okhotsk ice cover and its relation to oceanic processes, *J. Geophys. Res.*, *92*(C12), 13,013–13,028.

Aota, M., and M. Ishikawa (1991), Fresh water supply to the Sea of Okhotsk and volume transport of Soya Warm Current, *Bull. Hokkaido Natl. Fish. Res. Inst.*, *55*, 109–113.

Cavalieri, D. (1994), A microwave technique for mapping thin sea ice, *J. Geophys. Res.*, *99*(C6), 12,561–12,572.

Drucker, R., S. Martin, and R. Moritz (2003), Observations of ice thickness and frazil ice in the St. Lawrence Island polynya from satellite imagery, upward looking sonar, and salinity/temperature moorings, *J. Geophys. Res.*, *108*(C5), 3149, doi:10.1029/2001JC001213.

Egbert, G. D., and R. D. Ray (2000), Significant dissipation of tidal energy in the deep ocean inferred from satellite altimeter data, *Nature*, *405*, 775–778.

Gawarkiewicz, G., and D. Chapman (1995), A numerical study of dense water formation and transport on a shallow, sloping continental shelf, *J. Geophys. Res.*, *100*(C3), 4489–4507.

Gladyshev, S., S. Martin, S. Riser, and A. Figurkin (2000), Dense water production on the northern Okhotsk shelves: Comparison of ship-based spring-summer observations for 1996 and 1997 with satellite observations, *J. Geophys. Res.*, *105*(C11), 26,281–26,299.

Gladyshev, S., L. Talley, G. Kantakov, G. Khen, and M. Wakatsuchi (2003), Distribution, formation, and seasonal variability of Okhotsk Sea Mode Water, *J. Geophys. Res.*, *108*(C6), 3186, doi:10.1029/2001JC000877.

Kampf, J., and J. O. Backhaus (1998), Shallow, brine-driven free convection in polar oceans: Nonhydrostatic numerical process studies, *J. Geophys. Res.*, *103*(C3), 5577–5593.

Kimura, N., and M. Wakatsuchi (1999), Processes controlling the advance and retreat of sea ice in the Sea of Okhotsk, *J. Geophys. Res.*, *104*(C5), 11,137–11,150.

Kitani, K. (1973), An oceanographic study of the Okhotsk Sea–Particularly in regard to cold waters, *Bull. Far Seas Fish. Res. Lab.*, *9*, 45–76.

Kowalik, Z., and I. Polyakov (1998), Tides in the Sea of Okhotsk, *J. Phys. Oceanogr.*, *28*, 1389–1409.

Martin, S., R. Drucker, and K. Yamashita (1998), The production of ice and dense shelf water in the Okhotsk Sea polynyas, *J. Geophys. Res.*, *103*(C12), 27,771–27,782.

Maslanik, J., and J. Stroeve (2003), DMSP SSM/I daily polar gridded brightness temperatures (updated) [CD-ROM], Natl. Snow and Ice Data Cent., Boulder, Colo.

Moroshkin, K. V. (1968), *Water Masses of the Sea of Okhotsk*, U.S. Dep. of Comm. Joint Publ. Res. Serv., Washington, D. C.

Ohshima, K., D. Simizu, M. Itoh, G. Mizuta, Y. Fukamachi, S. Riser, and M. Wakatsuchi (2004), Sverdrup balance and the cyclonic gyre in the Sea of Okhotsk, *J. Phys. Oceanogr.*, *34*, 513–525.

Schott, F., and W. Johns (1987), Half-year-long measurements with a buoy-mounted acoustic Doppler current profiler in the Somali Current, *J. Geophys. Res.*, *92*(C5), 5169–5176.

Schott, F., M. Visbeck, and J. Fischer (1993), Observations of vertical currents and convection in the central Greenland Sea during the winter of 1988–1989, *J. Geophys. Res.*, *98*(C8), 14,401–14,421.

Shcherbina, A. Y., L. D. Talley, and D. L. Rudnick (2003), Direct observations of North Pacific ventilation: Brine rejection in the Okhotsk Sea, *Science*, *302*(5652), 1952–1955.

Shcherbina, A. Y., L. D. Talley, and D. L. Rudnick (2004), Dense water formation on the northwestern shelf of the Okhotsk Sea: II. Quantifying the transports, *J. Geophys. Res.*, *109*, C09S09, doi:10.1029/2003JC002197, in press.

Simpson, J. H. (1981), The shelf-sea fronts: Implications of their existence and behaviour, *Philos. Trans. R. Soc. London, Ser. A*, *302*(1472), 531–543.

Simpson, J. H., and J. R. Hunter (1974), Fronts in the Irish Sea, *Nature*, *250*, 404–406.

Talley, L. D. (1991), An Okhotsk water anomaly: Implications for ventilation in the North Pacific, *Deep Sea Res.*, *38*, Suppl. 1, S171–S190.

Ullman, D. S., A. C. Dale, D. Hebert, and J. A. Barth (2003), The front on the northern flank of Georges Bank in spring: 2. Cross-frontal fluxes and mixing, *J. Geophys. Res.*, *108*(C11), 8010, doi:10.1029/2002JC001328.

Ushio, S., and M. Wakatsuchi (1993), A laboratory study on supercooling and frazil ice production processes in winter coastal polynyas, *J. Geophys. Res.*, *98*(C11), 20,321–20,328.

Wilson, C. D., and E. Firing (1992), Sunrise swimmers bias acoustic Doppler current profiles, *Deep Sea Res.*, *39*, 885–892.

Yasuda, I. (1997), The origin of the North Pacific Intermediate Water, *J. Geophys. Res.*, *102*(C1), 893–909.

D. L. Rudnick, A. Y. Shcherbina, and L. D. Talley, Scripps Institution of Oceanography, University of California, San Diego, 9500 Gilman Drive, La Jolla, CA 92093-0230, USA. (ashcherbina@ucsd.edu)